IEEE Access
Multidisciplinary ⋮ Rapid Review ⋮ Open Access Journal

Received 25 July 2023, accepted 25 August 2023, date of publication 5 September 2023, date of current version 13 September 2023.

Digital Object Identifier 10.1109/ACCESS.2023.3312180

RESEARCH ARTICLE

Designing a New Controller in the Operation of the Hybrid PV-BESS System to Improve the Transient Stability

MOHANA ALANAZI[1], MOHAMED SALEM[2], (Member, IEEE), MOHAMMAD HOSEIN SABZALIAN[3], NATARAJAN PRABAHARAN[4], (Senior Member, IEEE), SOICHIRO UEDA[5], (Student Member, IEEE), AND TOMONOBU SENJYU[5], (Fellow, IEEE)

[1]Department of Electrical Engineering, College of Engineering, Jouf University, Sakaka 72388, Saudi Arabia
[2]School of Electrical and Electronic Engineering, Universiti Sains Malaysia (USM), Nibong Tebal, Penang 14300, Malaysia
[3]Department of Mechanical Engineering, Faculty of Engineering, University of Santiago of Chile (USACH), Santiago 9170022, Chile
[4]Department of EEE, SASTRA Deemed to be University, Thanjavur, Tamil Nadu 613401, India
[5]Faculty of Engineering, University of the Ryukyus, Nakagami 903-0213, Japan

Corresponding authors: Mohana Alanazi (msanazi@ju.edu.sa), Tomonobu Senjyu (b985542@tec.u-ryukyu.ac.jp), and Natarajan Prabaharan (prabaharan.nataraj@gmail.com)

This work was supported by the Deputyship for Research and Innovation, Ministry of Education in Saudi Arabia, under Project 223202.

ABSTRACT The main aim of this paper is to design a local controller for DC/DC converter in a battery energy storage system (BESS) and a controller based on a virtual synchronous generator (VSG) for photovoltaic (PV) converter connected to AC grid. In the DC/DC converter design, the state feedback method is used so that the voltage and current control loops are combined, leading to higher flexibility and improved damping. This flexibility, which maintains the state of charge (SOC) of BESS, is supported by the design of virtual resistance and virtual capacitor statically and dynamically. In this design method, the BESS can be independently connected to each DC bus node and detect disturbances through local measurements. In addition, the improved Pre-Parallelism (PREP) method has been used to improve the transient performance caused by the disconnection and connection of additional loads, the existence of faults, and the inherent inertia difference in parallel operation between VSG and synchronous generator (SG). In this method, the problem of phase jump caused by transient disturbances is solved by considering a cosine function in VSG design. Also, to solve the problem of inertia difference between the units, a small signal model has been presented, in which, by considering the capacity ratio of the units on the AC side, the necessary inertia for VSG can be included in the design. The proposed method is simulated by considering different scenarios in MATLAB software, so the results demonstrate the superiority of the proposed controller compared to other existing methods.

INDEX TERMS Microgrid, energy, battery energy storage system, virtual synchronous generator, photovoltaic, state feedback.

I. INTRODUCTION

One of the most essential energy-related challenges recently is the widespread development of renewable energy sources (RES) to provide sustainable and environmentally friendly energy [1]. Therefore, achieving such a scenario requires an evolution in energy management because power generation planning results from system flexibility [2], [3], [4]. This is seen with numerous initiatives for international projects to offer flexibility in the generation, transmission [5], distribution, and consumption of electricity [6], [7]. In this regard, the most promising concept for integrating RES sources in hybrid energy flexibly and efficiently is presented as a microgrid (MG) [8], [9]. Among the types of RES used to start MGs, PV equipped with BESS has received more attention in rural areas far from the grid or the possible islanding phenomenon

The associate editor coordinating the review of this manuscript and approving it for publication was Alfeu J. Sguarezi Filho.

This work is licensed under a Creative Commons Attribution-NonCommercial-NoDerivatives 4.0 License.
For more information, see https://creativecommons.org/licenses/by-nc-nd/4.0/

due to self-compensation [10], [11]. In addition, due to the production of DC electricity by PV-BESS, it can be used more economically in the distribution of DC energy to charge electric vehicles, household devices, telecommunication towers, and data centers [12], [13]. In [14], to improve the fluctuations caused by wind and PV energy, a BESS station is used to adjust BESS power levels based on the variations of the units and the SOC levels.

Similarly, in [15], this setting is presented based on direct power control with droop rate in PV. In the mentioned methods, the dynamic model of the system is unknown during the design of the controller, which is considered a negative factor from the point of view of stability. In [16], the control design for the PV converter using the droop method is presented in more detail to increase the PV power during disturbances. However, the design of the BESS-related controller to measure the PV output power requires online measurements, which leads to the difficult location of the BESS. As a result, to solve this problem, a high-speed communication link should be used in the design, which in addition to increasing the operating cost, also makes the design process more difficult. In [17], the emulation of a virtual capacitor is used to compensate the inertia required for droop gain based on the SOC of the BESS. The mentioned method does not perform appropriately in weak grids due to the use of proportional-integral (PI) controllers in voltage and current loops.

At present, most RESs are operated in AC grid-connected mode with grid-imposed voltage and frequency and inject a predefined amount of power into the grid [18], [19], [20]. In the island operation mode, the MG should adjust the voltage and frequency within the determined limits while maintaining the power balance [21]. In this regard, using a set of droop topologies without inertia reduces the reliable performance of MGs [22]. Therefore, in order to operate RES more safely, their DC/AC converter can be controlled through a VSG. In this case, by simulating the governor control in traditional power stations, which is referred to as droop control, it is possible to simulate the inertia of the rotating machine or the oscillating equation of the synchronous generator, which is called VSG [23]. In this regard, the use of different controllers to support the MG frequency requires energy storage. In the wind power plant, the kinetic energy stored in the rotor blade can be used as an energy source to support this frequency [24]. But in the PV system, since there is no rotating part and the only energy storage elements include the DC link capacitor and the inductance of the converters, for this reason, the stored energy of the DC link capacitor in the PV inverter is used to support the MG (through virtual inertial control (VIC)) frequency in the switching reference signals [25]. An alternative method for frequency support is a load-shedding strategy where the PV operates away from its maximum power point. In this method, the difference between the maximum available power and absorbed power can be used as reserve power to support MG frequency during disturbances. The main advantage of load shedding is the lack of additional investment in additional and complex control elements [26]. In [27], an optimal control method based on reinforcement learning is proposed for the three-phase grid-connected inverter used in VSGs. In this case, the dynamics of the system are unknown under different operating conditions of the grid, including balanced/unbalanced networks and the presence of voltage drop in weak grids. The mentioned method is only designed for a DC/AC converter, and RES and BESS modeling is not used for MG frequency support. In [28], the dynamic characteristics of energy storage considering SOC time have been used for VSG control. So that the neural network based on Radial Basis Function (RBF) can be used to learn the data features and the nonlinear relationship between the input voltage and the output power of the energy storage. The mentioned method is only designed based on the dynamic characteristics of the inverter, and there is no energy management on the BEES charge and discharge modes. In [29], using the Kalman filter method, first the BESS charge and discharge status is estimated online, and then the droop and inertia parameters are designed through fuzzy logic and smart algorithms based on the battery status and bus voltage deviation. However, the static and dynamic characteristics of BESS to make the network more stable are not available in the controller design, and the controller performance is poor for supporting DC loads. In [30], in order to solve the problem of voltage fluctuations caused by distributed generation (DG), a coordinated voltage and frequency deviation controller has been used in a group of BESS installed on the feeder of the distribution network. So that when the feeder is isolated due to a fault, the frequency deviation controller based on the hysteresis loop activates the frequency control loop to control the frequency and voltage of the island synchronously to realize the self-healing of the island. In the mentioned paper, BESS is modeled as a DC source, and therefore no controller is proposed on the SOC level, and the battery is connected to the AC grid through an inverter, which eliminates the scenario of feeding DC loads on the battery side. In [31], the optimal voltage and frequency recovery method based on decentralized state estimation is used to control the inverter of distributed energy resources (DER). In the mentioned method, the reference signal related to the primary controller is optimally predicted so that it is not affected by the local measurement noise, so the shared power between DERs is guaranteed. In [32], the Model Predictive Controller (MPC) method is also presented to control the DC/AC converter in BESS. The mentioned method provides inertial support in transient states and increases the dynamic characteristics of voltage and frequency of the system. By creating a prediction model in the signals related to the VSG controller (including frequency and power), the required active and reactive power increase is calculated and then placed on the VSG power reference. In [31] and [32], in order to obtain optimal signals, it is necessary to have an accurate system model. In addition, if the DERs model is considered dynamically, it will lead to the complexity of the cost function in MPC, which makes the implementation of the control process more difficult. By studying the above research, it is clear that their

TABLE 1. Comparison of relevant literature around stability improvement of local controller for DC/DC converter in BESS and controller VSG for PV converter connected to AC grid.

Issue	Reference										
	[17]	[18]	[19]	[21]	[22]	[23]	[24]	[28]	[29]	[41]	This paper
Designing the independent BESS controller to measure local disturbances	✓	✓	×	✓	×	✓	×	✓	×	×	✓
Dynamic and static support in BESS at the same time for coordination and optimal management of energy with other renewable sources	×	×	×	×	✓	×	✓	×	✓	×	✓
Optimum designs of full state feedback controller	×	×	×	×	×	×	✓	×	×	×	✓
Improved PREP design to compensate for phase angle jump	×	×	×	×	×	×	×	×	×	✓	✓
Inertia matching and active power appropriation between VSG and SG units	×	×	✓	×	×	✓	×	×	✓	×	✓

focus is related to DC/AC converter control only for parallel VSGs. But when the SGs are disconnected, the stability of the system may be affected due to the difference between the moment of inertia and the inertia of the main driving axis for the VSG and SG units and cause transient oscillations. So that these fluctuations affect the speed of the SG rotor and reduce the capacity of power appropriation between the units, in addition, in extreme conditions, it may cause system instability. In [33] and [34], the difference in inertia between inverters and SGs has been analyzed concerning frequency fluctuations and weak transient power sharing. However, operation in such conditions will lead to stability problems caused by transient conditions due to the non-integration of the model and system parameters. In [35], a specific configuration of VSG is proposed to improve performance due to transient conditions under load changes, while the capacity appropriation ratio of VSG and SG is not considered. In [36], transient virtual impedance is added to VSGs to reduce SG rotor speed deviation under unbalanced load operation. Meanwhile, the difference in the speed deviation response causes the instability of the point of common coupling (PCC) voltage, which ultimately causes high frequency fluctuations in the output power. However, the parallel operation characteristics of VSGs and SGs have not been considered. In this regard, one of the methods of reducing phase disturbances in the synchronization of the inverter connected to the grid is the use of virtual impedance in VSG [37]. In this work, the ideas proposed for the PREP method in paralleling the VSG with the SG are without considering the effect of the LC filter, which causes voltage phase deviations. Also, a PREP method in VSG is based on virtual power and secondary control of voltage and frequency, in which phase synchronization must be done after secondary control, while this method causes irregular signal adjustment [38]. In the traditional methods related to PERP, by adding phase difference to the frequency control loop by a PI controller, the phase jump is somewhat improved [39]. However, the phase jump in cases where the system dynamics is slow may lead to PERP failure, which reduces the reliability of network operation. After reviewing the previous works, the features of the related literature can be summarized as Table 1.

Based on the above research, the main aim of this paper is to design controllers for BESS and VSG parallelized with SG. The suggested controller for BESS employs the idea of virtual capacitor emulation and droop controller to deliver static and dynamic support. Therefore, unlike the usual methods where the design is done separately between the voltage and current loops, a full-state feedback controller is used in the suggested method, so that optimal design can be done by integrating the voltage and current loops. In addition, a new and improved PREP-based method is proposed to eliminate the effect of phase angle jump on the transient electromagnetic performance of MGs in parallel operation of VSG with SG. Also, the design of VSG parameters considering the matching of inertia between units has been analyzed based on the small signal model. In short, the innovations of this article are as the following:

- Designing the independent BESS controller to measure local disturbances and provide the necessary support to maintain energy management in the network.
- Dynamic and static support in BESS at the same time for coordination and optimal management of energy with other renewable sources.

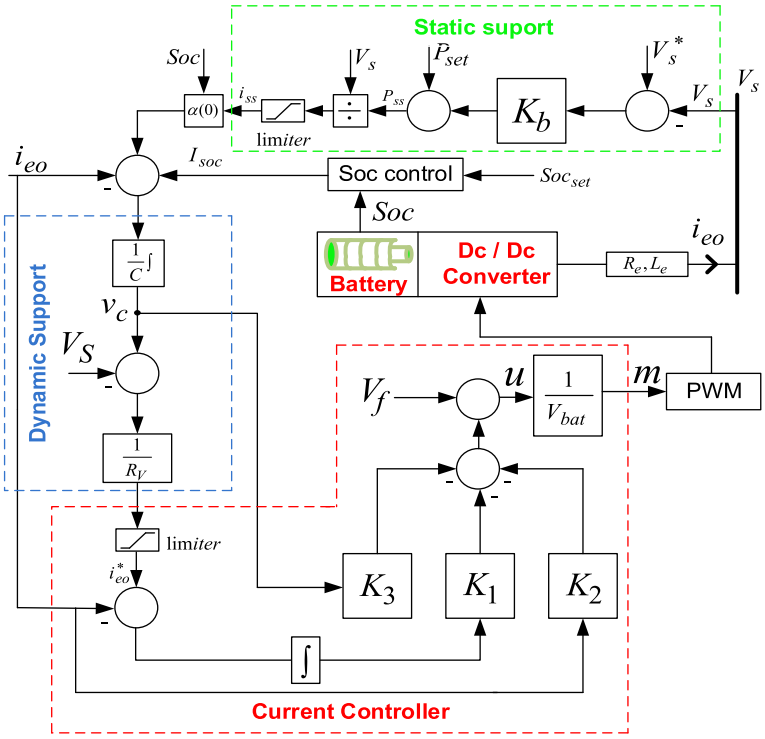

FIGURE 1. Structure of the BESS connected to DC grid.

- Optimum designs of full state feedback controller in order to robust the proposed method due to disturbances.
- Improved PREP design to compensate for phase angle jump in parallel operation of SG with VSG.
- Inertia matching and active power appropriation between VSG and SG units based on the small signal model.

II. PROPOSED CONTROLLER MODELING PROCESS FOR BESS

A. BATTERY STORAGE SYSTEM MODEL AND RELATED CONTROLLER

Figure 1 shows the control block diagram of a BESS linked to the DC grid, where v_s and i_{eo} are the dc bus voltage and the output current in the bidirectional dc/dc converter, respectively. In this structure, if a disturbance occurs in the DC grid, the proposed design detects it and provides the desired response according to the severity of the disturbance. This answer is used in two parts for DC network support:

- The first part is related to the dynamic response support based on the inertia created by a capacitor with capacitance C.
- The second part concerns the static support generated through a droop controller by the term $K_b(V_s^* - V_s)$, where V_s^* is the nominal value of V_s. In the proposed controller structure, by limiting the current of the converter, it can be protected against low voltage ride through (LVRT) and thus maintain the SOC level of the battery in an optimal state. For a voltage source converter (VSC), if $m(t)$ is defined as the modulation index and V_e as the battery voltage, the average battery output voltage can be defined as $v_{eo}(t) = m(t)V_e$ and the controller input as $u(t) = m(t)V_{be}$. Therefore, the following equation is obtained

$$\frac{d}{dt}i_{eo}(t) = -\frac{R_e}{L_e}i_{eo}(t) + \frac{1}{L_e}u(t) - \frac{1}{L_e}V_s(t) \tag{1}$$

L_e and R_e are the inductance and parasitic resistance of the filter, respectively.

Figure 2 shows the mathematical model of BESS based on the signal-averaging model in a switching cycle. To support the dynamic response in the dc grid, a capacitor with capacity C is used, whose mathematical model is described as (2):

$$I^* - i_{eo} = C\dot{v}_c \tag{2}$$

where $I^* = \alpha(i_{ss}, SOC) + I_{soc} = i_{set} + I_{soc}$ is obtained by the outer loops shown in Figure 2. It can be seen from Figure (2) that the grid voltage V_s and capacitor voltage V_c must be coupled to support the dc grid voltage. The mathematical equation of this voltage loop is described as (3):

$$V_c - V_s = i_{eo}^* R_v \tag{3}$$

where the resistance R_v is a positive constant. Also, since the changes in the current control loop occur rapidly, the resulting output current i_{eo} equates i_{eo}^* on the time scale of the voltage loop. With these descriptions, it can be said that in relation (3), R_v represents a virtual resistance between virtual capacitor C

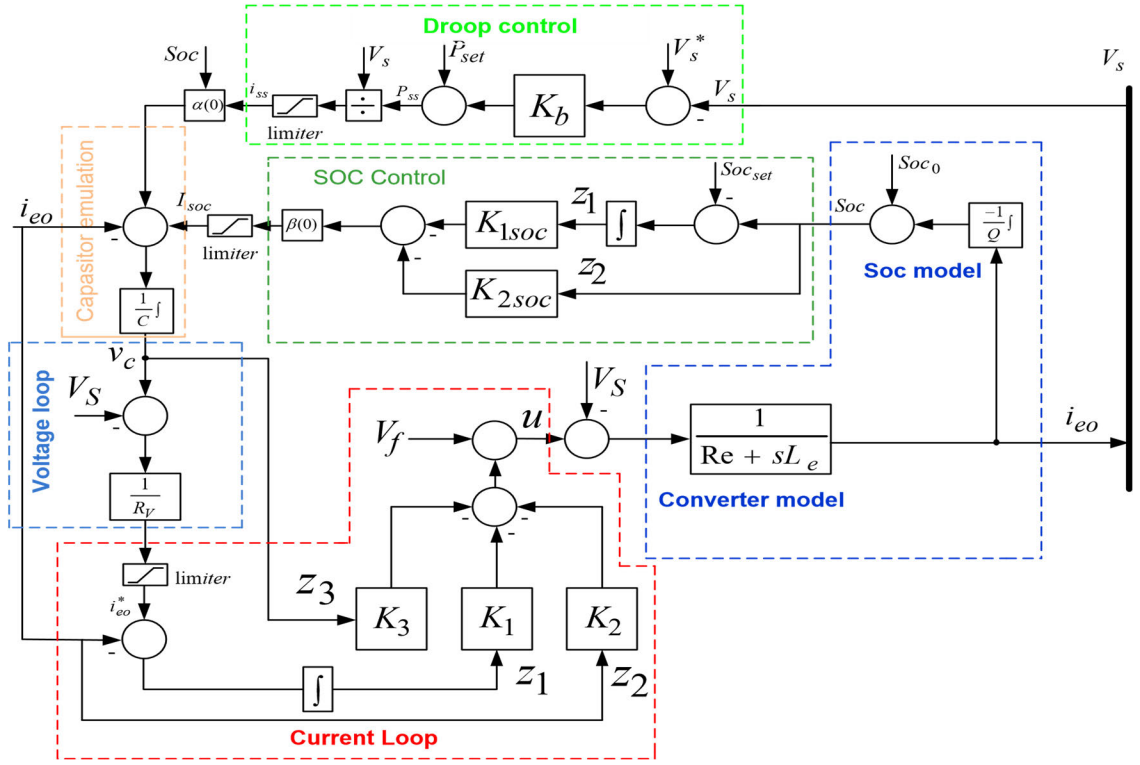

FIGURE 2. Proposed controller structure for BESS connected to DC grid.

and dc voltage. The static support of the dc grid, which is performed by the droop function, is expressed as (4):

$$P_{ss} = P_{set} + K_b(V_s^* - V_s) \tag{4}$$

where K_b and P_{set} represent droop gain and power set point, respectively. In order to reduce the measurement error of the i_{eo} converter current compared to the reference value i_{eo}^*, the changes must be fast, for this purpose the use of a full state feedback controller with gains K_1, K_2 and K_3 is required. Mathematically, SOC charge level is defined as follows (5):

$$SoC(t) = SoC_0 - \frac{1}{Q}\int_0^t i_{eo}(t)dt \Rightarrow \frac{d}{dt}SoC(t) = -\frac{1}{Q}i_{eo}(t) \tag{5}$$

where SoC_0 is the initial value of SOC and Q is the charge capacity in unit ampere-second. In the proposed structure of Figure 2, in order to reach SOC_{set}, it is necessary that the controller related to SOC generates the incremental current of I_{soc}. In this structure, the parameter β is used to adjust the control strength in SOC and the parameter α is used to adjust the SOC level statically.

B. DESIGN OF VIRTUAL CAPACITOR C AND VIRTUAL RESISTANCE RV

The dynamic power produced by the capacitor is expressed as (6):

$$P_{dyn} = -CV_c\frac{dV_c}{dt} \approx -CV_s\frac{dV_s}{dt} \approx -CV_s^*\frac{dV_s}{dt} \tag{6}$$

When an actual capacitor is directly linked to the dc bus, the voltage is equal to the dc grid voltage, which leads to zero resistance. But in order for the controller to track the signals optimally, it is necessary to design a non-zero resistance in the form of R_v. For an RC circuit, the cutoff frequency is equal to $f_c = 1/2\pi R_v C$ with accordingly, in order to achieve a large bandwidth; the value of R_v should be small enough. On the other hand, a very small value of R_v leads to the amplification of sounds and strong jumps in V_s, accordingly, the value of R_v chosen in this paper is between 0.01 and 0.1 per unit to meet the above requirements.

C. DESIGN OF BESS GAIN CONTROLS

1) GAIN DESIGN RELATED TO DROOP CONTROLLER

In this paper, the adjustment factor of droop controller is considered as $K_b = P_{rated}/\Delta V_s$. where P_{rated} is the rated power of the BESS and ΔV_s is the permissible variation of the dc bus voltage. To limit the transient voltage, module's output is passed through a limiter.

2) DESIGNING THE GAINS RELATED TO THE CURRENT CONTROLLER

For the purpose of optimal operation, the linear quadratic regulator (LQR) method has been used to design the gains of the controllers. According to Figure 2, it is assumed to be $z_1(t) = \int e(t)dt = \int(-i_{eo}(t) + i_{eo}^*(t))dt$, $z_2(t) = i_{eo}(t)$ and $z_3(t) = V_c(t)$. Therefore, the following equations are

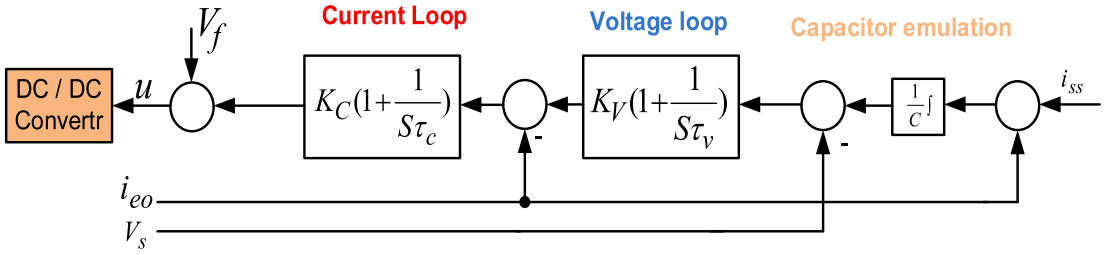

FIGURE 3. The structure of the BESS controller in the traditional method.

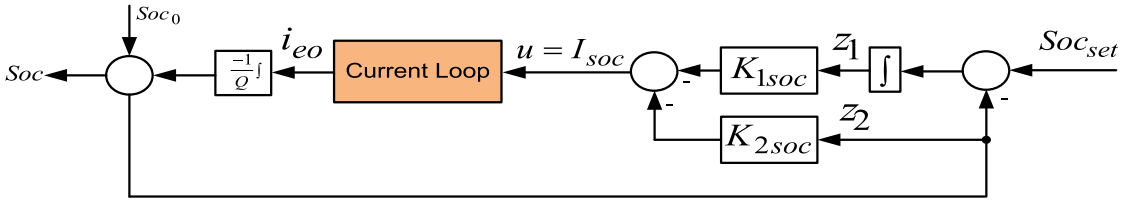

FIGURE 4. The structure of the SOC controller.

followed:

$$\begin{cases} \dot{z}_1 = -z_2 + \dfrac{z_3}{R_v} - \dfrac{V_s}{R_v} \\ \dot{z}_2 = -\dfrac{R_e}{L_e} z_2 + \dfrac{u}{L_e} - \dfrac{V_s}{L_e} \\ \dot{z}_3 = -\dfrac{z_2}{C} + \dfrac{i_{ss}+I_{SOC}}{C} \\ u = -K_1 z_1 - K_2 z_2 - K_3 z_3 + V_f \end{cases} \tag{7}$$

where the constant term $V_f = V_s(0)+K_3V_c(0)$ is used for a soft start. where $V_s(0)$ is used as a substitute for the filtered version of the dc grid voltage in order to improve the current limit. The purpose of this substitution is to be able to track z_2 by its reference in the presence of perturbation. This approach leads to robust tracking of signals that, by applying a d/dt differential on both sides of equation (7), an LQR can be achieved. Therefore, the following equations are obtained (8):

$$\begin{cases} \dot{x}_1 = -x_2 + \dfrac{z_3}{R_v} \\ \dot{x}_2 = -\dfrac{R_e}{L_e} z_2 + \dfrac{1}{L_e} w \\ \dot{x}_3 = -\dfrac{z_2}{C} \\ w = -K_1 x_1 - K_2 x_2 - K_3 x_3 \end{cases} \tag{8}$$

where is $x_i(t) = \dot{z}_i(t)$ and $w(t) = \dot{u}(t)$. Considering that i_{ss} and I_{SOC} have slower dynamics and the voltage V_s is a dc value, therefore the differential $dV_s/dt = di_{ss}/dt = dI_{soc}/dt = 0$. Based on this, the set of equation (8) is defined as (9):

$$\begin{cases} \dot{z}(t) = Az(t) + Bw(t) \\ w(t) = -Kz(t) \end{cases} \tag{9}$$

where:

$$A = \begin{bmatrix} 0 & -1 & \frac{1}{R_v} \\ 0 & -\frac{R_b}{L_e} & 0 \\ 0 & -\frac{1}{C} & 0 \end{bmatrix}, B = \begin{bmatrix} 0 \\ \frac{1}{L_e} \\ 0 \end{bmatrix}, K = \begin{bmatrix} K_1 \\ K_2 \\ K_3 \end{bmatrix}^T \tag{10}$$

With the purpose of adjusting the controller gains to BESS, an objective function has been defined according to equation (10) so that the measurement error of control signals can be considered as $x_1(t) = e(t)$. And therefore, by placing x_1 with measurement error signal, we seek to direct this error signal to zero obtain more accurate controlled gain. So with the aim of setting $x_1(t) = e(t)$ to zero value, the objective function is defined as (11):

$$J = \int_0^\infty [S_1 e^2(t) + S_2 x_2^2(t) + S_2 x_3^2(t) + w^2(t)]dt \tag{11}$$

In order to achieve a fast and smooth response in the regulation of the current controller, the S_i parameters in the K design can be systematically adjusted [40]. According to the traditional method presented in Figure 3, the voltage and current loops are designed separately, and there is no K_3 branch, which leads to the voltage loop being slower than the current loop. A further explanation is that in the traditional structure of the controller design, it forces the current loop to have a vast bandwidth, which requires the bandwidth margin of the voltage loop to be large to allow the bandwidth to pass to the current loop. But the larger margin of bandwidth in the voltage loop may cause excessive PWM modulation throughout the transient period. But in the proposed plan, by adding a feedback loop with K_3 gain, which includes virtual capacity (C) and virtual resistance (R_v), both loops can be integrated and the bandwidth problem can be solved. This structure leads to more flexibility in the selection of R_v, whereby the speed and damping of responses in the controller increases.

3) DESIGNING THE GAINS RELATED TO THE SOC CONTROLLER

According to the SOC control structure shown in Figure 4, we first assume $z_2(t) = SoC(t), z_1(t) = \int(-SoC(t) + SoC_{set})dt$ and $u(t) = I_{soc}(t)$. Therefore, the

state equations are expressed as (12):

$$\begin{cases} \dot{z}_1 = -z_2 + SoC_{set} \\ \dot{z}_2 = -\dfrac{1}{Q}u + \dfrac{u}{L_e} - \dfrac{V_s}{L_e} \\ u = -K_{1soc}z_1 - K_{2soc}z_2 \end{cases} \tag{12}$$

To track the reference z_2 in the presence of disturbance, by applying a differential d/dt to both sides of equation (12), we can achieve the solution of an LQR-based problem, which is expressed as (13):

$$\begin{cases} \dot{x}_1 = -x_2 \\ \dot{x}_2 = -\dfrac{1}{Q}w \\ w = -K_{1soc}x_1 - K_{2soc}x_2 \end{cases} \tag{13}$$

By rewriting relation (13) as a set of state equations as $x_i = \dot{z}_i$ and $w = \dot{u}$, we can express (14):

$$\begin{cases} x(t) = Ax(t) + Bw(t) \\ w(t) = -Kx(t) \end{cases} \tag{14}$$

where:

$$A = \begin{bmatrix} 0 & -1 \\ 0 & 0 \end{bmatrix}, B = \begin{bmatrix} 0 \\ -\frac{1}{Q} \end{bmatrix}, K = \begin{bmatrix} K_{1soc} \\ K_{2soc} \end{bmatrix} \tag{15}$$

With the aim of setting $x_1(t) = e(t)$ to zero value, the objective function is defined as (16):

$$J = \int_0^\infty [S_1 e^2(t) + S_2 x_2^2(t) + w^2(t)]dt \tag{16}$$

4) ADJUSTMENT FACTOR (β) FOR SOC

By defining the regulation coefficient β for SOC charge and discharge, we will have (17):

$$\beta = \begin{cases} 1 & SoC_a < SoC < SoC_b \\ 1 + \chi\,|SoC - SoC_{set}| & otherwise \end{cases} \tag{17}$$

where the coefficient χ is a positive constant. In other words, this coefficient adjusts the distance between the actual SOC and the desired value.

5) STATIC SUPPORT ADJUSTMENT FACTOR (α)

In order to avoid the possible excessive discharge of SOC [41], the adjustment coefficient of the static supporter is expressed as (18):

$$\alpha = \begin{cases} 1 & \text{if } \begin{matrix} \mathrm{Vs} < \mathrm{V_s^*} \\ \text{and } \mathrm{SoC_a} \le \mathrm{SoC} \end{matrix} \\ \dfrac{\mathrm{SoC} - \mathrm{SoC_{min}}}{\mathrm{SoC_a} - \mathrm{SoC_{min}}} & \text{if } \begin{matrix} \mathrm{Vs} < \mathrm{V_s^*} \text{ and} \\ \mathrm{SoC_{min}} < \mathrm{SoC} < \mathrm{SoC_a} \end{matrix} \\ 0 & \text{if } \mathrm{Vs} < \mathrm{V_s^*} \text{ and } \mathrm{SoC_a} \le \mathrm{SoC}_{\ \mathrm{min}} \\ 1 & \text{if } \mathrm{Vs} \ge \mathrm{V_s^*} \text{ and } \mathrm{SoC} \le \mathrm{SoC_b} \\ \dfrac{SoC - SoC_{\mathrm{min}}}{SoC_a - SoC_{\mathrm{min}}} & \text{if } \begin{matrix} \mathrm{Vs} \ge \mathrm{V_s^*} \text{ and} \\ \mathrm{SoC_b} < \mathrm{SoC} < \mathrm{SoC_{max}} \end{matrix} \\ 0 & \text{if } \mathrm{Vs} \ge \mathrm{V_s^*} \text{ and } \mathrm{SoC_{max}} \le \mathrm{SoC} \end{cases} \tag{18}$$

where $\mathrm{SOC_{min}}$ and $\mathrm{SOC_{max}}$ are the min and max limits of the SOC level, respectively. Also, $\mathrm{SOC_a}$ and $\mathrm{SOC_b}$ are the upper and lower bounds in the static support level, respectively. For further explanation, it can be said that: beta coefficient is related to the state of charging and discharging of the battery, and alpha represents the coefficient to adjust the BESS static backup to avoid the possible excessive discharge of SOC. In other words, these two coefficients are used for BESS energy management.

III. MODELING PROCESS FOR GRID-CONNECTED INVERTER CONTROL BASED ON VSG

A. BASIC MODEL FOR VSG

Figure 5 shows the control block diagram for a VSG along with the active and reactive power loops, the virtual impedance module, and the modulation signals for the DC/AC converter. According to Figure 5, the initial modeling (without considering the PREP loop) for a VSG is expressed as [41] (19):

$$\begin{cases} P_v^* + D_{pv}(\omega_n - \omega) - P_e = J_v\omega_n\dfrac{d\omega}{dt} \\ Q_v^* + D_{qv}(V_n - V_0) - Q_e = K_v\dfrac{dE_m}{dt} \\ \delta_v = \displaystyle\int(\omega - \omega_n)dt \end{cases} \tag{19}$$

where P_v^* and Q_v^* are the reference active and reactive powers, D_{pv} and D_{qv} are respectively related to the active power frequency factor (P-ω) and the voltage droop factor related to the reactive power (Q-V), P_e and Q_e are the electromagnetic active and reactive powers, J_v and K_v are the virtual moment of inertia and voltage coefficient respectively, n_ω and ω are the nominal and actual rotor speed respectively, V_n and V_0 are the effective values of the nominal and actual voltage range respectively, E_m is the internal potential magnitude, and δ is the VSG power angle.

B. SYNCHRONOUS GENERATOR MODEL

Figure 5 shows that the SG controller includes a governor (GOV) and an automatic voltage regulator (AVR). So that the power of the main driving shaft $\mathrm{P_{ms}}$ is adjusted by GOV based on the angular frequency ω_s and ω_n. In order to model the delay in the response of the mechanical system, a loop with the first-order moment of inertia $1/(\tau_\mathrm{d}\ \mathrm{s}+1)$ has been used in the governor. Where τ_d is the time constant of intrinsic response, and K_G is the proportional coefficient of GOV. In the AVR loop, K_A is used as the droop coefficient, and the PI controller is used to adjust the field voltage V_{fs}. In order to coordinate the supply of the load on the PCC bus in the power system model, an SG is used as the main power supply. So that the PV inverter system is installed in parallel with SG and is controlled through VSG technology. In this design, as shown in Figure 5, when the breaker is open, AC loads are supplied only through SG, and when the breaker is closed, SG and VSG must share the right load power to maintain the stability of the whole system.

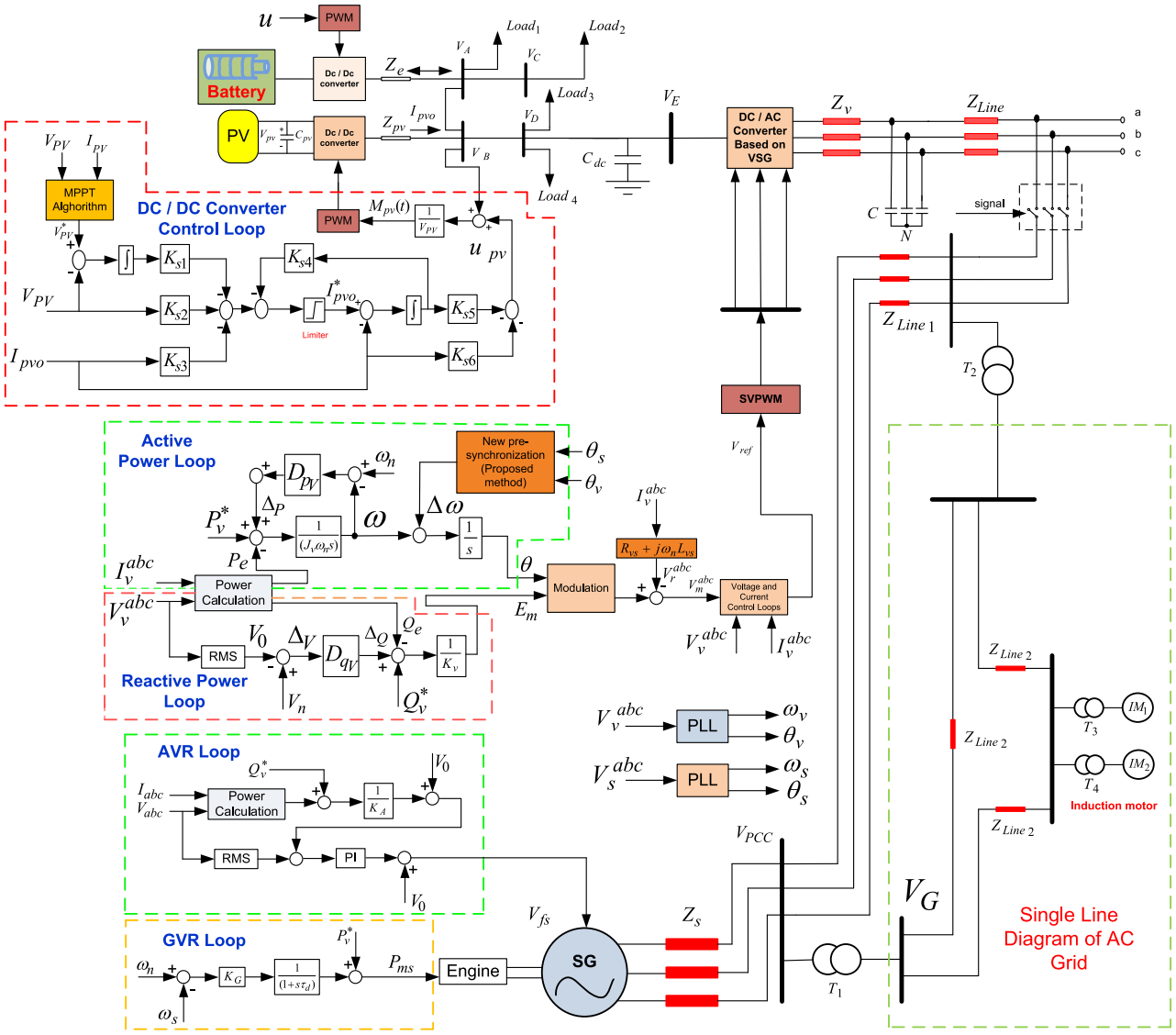

FIGURE 5. Block diagram of the MG under study with control loops.

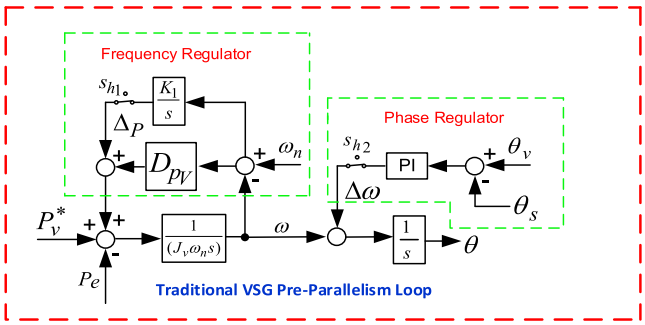

FIGURE 6. Traditional PREP controller structure.

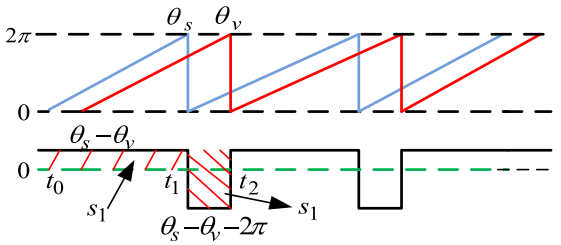

FIGURE 7. Phase jump difference curve.

C. PREP ALGORITHM

1) PHASE DIFFERENCE JUMP MODELING

In order to decrease the impact of electromagnetic and mechanical transients and also to ensure smooth operation in the VSG system, the instantaneous output voltage of VSG and SG should be constant and have the same characteristics such as amplitude, frequency and phase before the transient. The PREP method for VSG is similar to synchronization in a phase-locked loop (PLL) in grid-connected applications. For this purpose, according to Figure 6, in the traditional operating case, an integral controller K_1/s can be used to adjust the frequency difference and voltage amplitude, which is relatively simpler to implement [38].

With all these interpretations, the existence of transient states leads to the occurrence of phase jumps, which inevitably affects the performance of PREP and ultimately the maintenance of system stability. For better understanding, it can be said that the phase of a periodic signal, as shown in Figure 7, starts from 0 to 2π and 2π to 0 at the beginning of the cycle in the interval t_0 to t_1, and at the end of the cycle, a jump occurs in t_1 and the next cycle begins. It can be seen that the phase jump error remains during the period $t_1 \sim t_2$. Assuming that even the output voltage frequencies of SG and VSG are equal to each other and as $\omega_s = \omega_v$, the voltage phase (θ_s) of SG is pre-phase compared to the voltage phase (θ_v) of VSG, which is shown in Figure 7. As a result, these two phases in the synchronization process can never be exactly the same. In other words, in each cycle, the phase will have a positive and negative jump, which requires continuous forward and reverse adjustment of the output frequency. On the other hand, if we want to connect the phase signal directly to the VSG by the $\Delta\omega$ signal without considering the integrator, disturbances will occur in the power loop. Therefore, to solve the phase jump problem, without considering the integrator in Figure 6, the degree of phase adjustment can be expressed as (20):

$$\begin{aligned}\Delta\theta &= \int_{t_0}^{t_1} [\omega_v - \omega_s + k_d(\theta_s - \theta_v)]dt \\ &\quad + \int_{t_1}^{t_2} [\omega_v - \omega_s + k_d(\theta_s - \theta_v - 2\pi)]dt \\ &= k_d \left[\int_{t_0}^{t_2} (\theta_s - \theta_v)dt - 2\pi(t_2 - t_1) \right] \\ &= k_d(S_1 - S_2) \end{aligned} \tag{20}$$

where k_d is the proportionality factor of the phase controller. According to Figure 7, it can be seen that when $S_1 > S_2$, synchronization adjustment is achieved in a longer period of time. In the case $S_1 = S_2$, there is no change in the phase difference and phase synchronization is not achieved. And in the third case, when $S_1 < S_2$, the output phase of VSG is in a post-phase state until it is equal to the last cycle of the output phase of SG. As a result, it can be said that the PREP time is longer and even the system does not have the ability to synchronize. Even if PREP is fully parallelized and Sh_2 is opened according to Figure 6, removing the integrator unit from PI also affects the frequency stability of the system. Finally, it is concluded that the improvement of PREP should be ensured for the stability of the MG with SG and VSG units.

2) PROPOSED SCHEME OF PHASE SYNCHRONIZATION

In this section, based on the disadvantages of the classical method in the implementation of PREP, a new PREP method is used to neutralize the effect of phase angle jump. In this regard, considering that the values of cosine functions remain the same during phase jump between $\Delta\theta$ and $\Delta\theta$ - 2π. The cosine function can be used in the proposed design due to its uniformity and continuity in the range of [0, π] radians. For better understanding, according to Figure 8, it can be seen

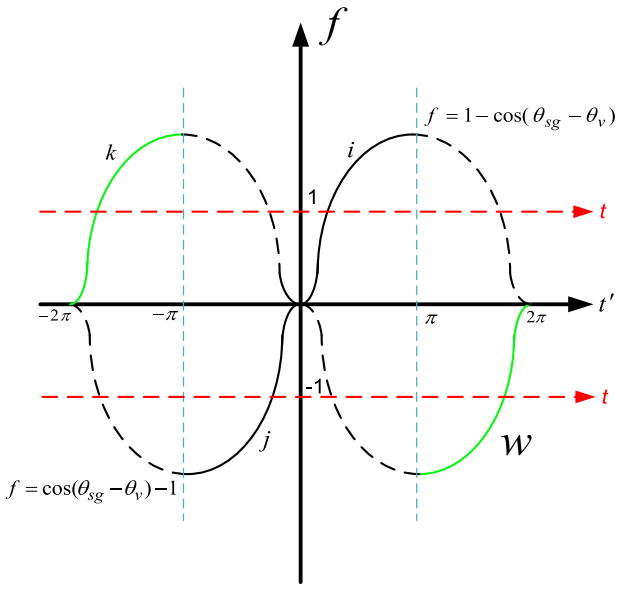

FIGURE 8. Phase transition curve for the proposed PREP method.

that a new function in the interval $0 \sim \pi$ is made as 1-cos(θ_s-θ_v) (line *i*) which, due to its non-negative value, can be a part of the post phase related to the phase SG compensated (line *j*). If this function continues, the phase range in $[-\pi, \pi]$ radians is also guaranteed. And if there is a jump in the phase difference, "*i*" and "*j*" lines will become "*k*" and "*w*" lines, respectively, without any change in its value or trend. Based on the above description and the function obtained by cosine functions, the frequency modulation signal can be expressed as (21):

$$\Delta\omega = \begin{cases} k_m[1 - \cos(\theta_s - \theta_v)] & 0 < \theta_s - \theta_v \le \pi \\ k_m[\cos(\theta_s - \theta_v)] & -1] \ -\pi < \theta_s - \theta_v \le 0 \\ k_m[1 - \cos(\theta_s - \theta_v - 2\pi)\,] & \\ -2\pi < \theta_s - \theta_v \le -\pi & \\ k_m[\cos(\theta_s - \theta_v + 2\pi) - 1 &] \ \pi < \theta_s - \theta_v \le 2\pi \end{cases} \tag{21}$$

where k_m is the modulation index in the interval $[-2\pi, 2\pi]$. By defining the relation (19), it is possible to prevent the negative effect of frequency and phase on the output voltage vector.

D. DESIGN VSG PARAMETERS

1) ADAPTATION OF INERTIAL PARAMETERS

Based on the explanation of the previous section and phase jump compensation, in this section, in order to improve the transient performance in VSG and SG paralleled with the grid, it should be possible to make a comparison between the damping and inertia parameters. In general, the small signal base model for a VSG can be defined as (22):

$$\begin{cases} J_v\omega_n s\Delta\omega_v = -\Delta P_v - D_{pv}\Delta\omega_v \\ s\Delta\delta_v = \Delta\omega_v \end{cases} \tag{22}$$

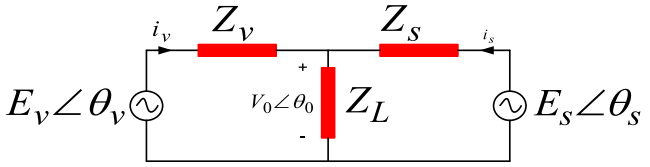

FIGURE 9. Circuit diagram of a microgrid based on SG and VSG in parallel operation mode.

where $\Delta\omega_v$ and $\Delta\delta_v$ are changes in angular frequency and power angle, respectively, and ΔP_v is changes in the active power of VSG. Also, for the small signal model in the SG speed loop, we will have (23):

$$J_s\omega_n s\Delta\omega_s = -\Delta P_s - \frac{K_G}{1+\tau_d s}\Delta\omega_s \tag{23}$$

where J_s is the moment of inertia, $\Delta\omega_s$ is the angular *frequency* and ΔP_s is the output power from SG. In the following, for the transfer functions (P-ω) related to VSG and active power loop SG, we will have (24)

$$\begin{cases} G_v = \dfrac{\Delta\omega_v}{\Delta P_v} = \dfrac{1}{-J_v\omega_n s - D_{pv}} \\ G_s = \dfrac{\Delta\omega_s}{\Delta P_s} = \dfrac{\tau_s s+1}{-J_s\omega_n\tau_d s^2 - J_s\omega_n s - K_G} \end{cases} \tag{24}$$

When s $\rightarrow$0, the corresponding droop coefficient depends on D_{pv} and k_p. Based on this, according to the capacity of the damping matching system, it is defined as (25):

$$\begin{cases} K_G S_s = D_{pv} S_v \\ K_A S_s = D_{qv} S_v \end{cases} \tag{25}$$

where S_s and S_v are the capacity of SG and VSG, respectively. According to relations (24) and (25), the transient performance of the grid is affected by the droop coefficients, the moment of inertia and the time constant of the initial response of the governor. Now, by defining the moment of inertia, we will have (26)

$$J_s = \frac{2HS}{\omega_n^2} \tag{26}$$

where H is known as the time constant of inertia and S is the capacity of the entire system. In order to ensure the improvement of the transient performance of the system, it should be possible to provide the desired H value for the system by using the inertial flexibility of the VSG. For this purpose, the equality of $\frac{J_s}{S_s} = \frac{J_v}{S_v}$ must be established to ensure the compatibility of the rotor inertia and the damping parameter.

2) REACTIVE POWER CONTROL

In general, the circuit model of VSG and SG can be considered equivalent to Figure 9. Where $E_v\angle\theta_v$ is the potential and VSG angle, $E_s\angle\theta_s$ potential and SG angle and $V_0\angle\theta_0$ are related to PCC bus voltage, Z_L is load impedance, Z_v and Z_s are VSG and SG system impedance, respectively. Based on this, according to Figure 9, the PCC bus voltage can be defined as (27):

$$V_0\angle\theta_0 = \frac{E_v\angle\theta_v + E_s\angle\theta_s}{Z\angle\theta_z} \tag{27}$$

where $z\angle\theta_z$ is the equivalent impedance in PCC bus. According to the inductive properties of SG and virtual impedance, the system impedance is assumed to be ideal (inductive), i.e. $Z_i = jX_i$. Based on this, the equivalent impedance can be expressed as (28):

$$\begin{cases} Z \\ = \left(\sqrt{(X_vX_sR_L)^2 + [(X_v+X_s)(R_L^2+X_L^2) + X_vX_sX_L]^2}\right) / \\ \left(X_vX_s(R_L^2+X_L^2)\right) \\ \theta_z = \tan^{-1}[-\dfrac{(X_v+X_s)(R_L^2+X_L^2)+X_vX_sX_L}{X_vX_sR_L}] \end{cases} \tag{28}$$

where R_L is the load resistance. Based on the instantaneous power theory, the active power Pv for VSG is defined as (29):

$$P_v = 3\times\left(\frac{E_v^2}{Z_v} - \frac{E_v^2}{Z_v^2 Z}cos\theta_z - \frac{E_vE_s}{Z_vZ_sZ}cos(\theta_z+\theta_v-\theta_s)\right) \tag{29}$$

Assuming that the system is ideal (inductive), the $\frac{\partial P_v}{\partial E_v} = \frac{\partial P_v}{\partial E_v} = 0$ equality holds. On the other hand, due to the small impedance angle difference, sin (θv-θs) will be equal to θ_v-θ_s and cos(θv-θs) will be equal to 1. Based on this, relation (29) is linearized as (30):

$$\begin{aligned} \Delta P_v &= M\,(\Delta\theta_v - \Delta\theta_s) = M\,[\Delta(\theta_v-\theta_0) - \Delta(\theta_s-\theta_0)] \\ &= M\,(\Delta\delta_v - \Delta\delta_s) \end{aligned} \tag{30}$$

where $M = E_vE_s sin\theta_z/(Z_vZ_sZ)$, δ_v and δ_s are the power angle of VSG and SG, respectively. Assuming that Y=[$\Delta\omega_v$, $\Delta\omega_s$]^T, N=[$\Delta\delta_v$, $\Delta\delta_s$]^T and also by inserting the relation (30) into (22), the MG state space model can be defined as (31):

$$\dot{Y} = \begin{bmatrix} \frac{-D_{pv}}{J_v\omega_n} & 0 & \frac{-M}{J_v\omega_n} & \frac{M}{J_v\omega_n} \\ 0 & \frac{-K_G}{J_s\omega_n+J_s\omega_n+\tau_d s} & \frac{M}{J_s\omega_n} & \frac{-M}{J_s\omega_n} \end{bmatrix} \begin{bmatrix} Y \\ N \end{bmatrix} \tag{31}$$

where Y and N are state vectors, by arranging relation (31), the following equation is obtained (32):

$$\dot{Y} + \begin{bmatrix} \frac{-D_{pv}}{J_v\omega_n} & 0 \\ 0 & \frac{-K_G}{J_s\omega_n+J_s\omega_n+\tau_d s} \end{bmatrix} + Y = \frac{M}{\omega_n}\begin{bmatrix} \frac{-1}{J_v} & \frac{1}{J_v} \\ \frac{1}{J_s} & \frac{-1}{J_s} \end{bmatrix} N \tag{32}$$

Equation (32) shows that when the moment of inertia and damping match, the power angle VSG and SG are coupled, which leads to the stability of the output frequency. Considering that the degree of instability of the system is strengthened by the inertia of the governor, by using the relation (22), which is the relationship between the output frequency and the power angle, the power angle signal can be adjusted during the transient period. Based on the fact that the capacity

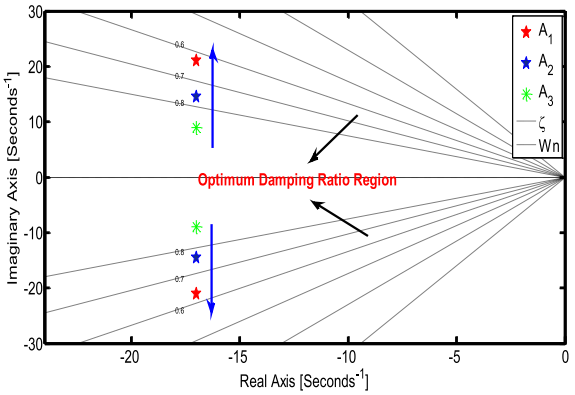

FIGURE 10. Location of closed loop system poles in the MG under study.

ratio is $S_v/S_s = n$, so from (25) and (28), it can be seen that $J_v/J_s = K_G/D_{pv} = n$, and as a result, by subtracting the active power loop in small signal models VSG and SG relative to each other, relation (33) is provided

$$\begin{aligned}\Delta P_s - \Delta P_v &= J_s\omega_n s(n\Delta\omega_v - \Delta\omega_s) + \frac{D_{pv}}{n}n\Delta\omega_v \\ &- \frac{K_G}{1+\tau_d s}\Delta\omega_s = \left(J_s\omega_n s + \frac{D_{pv}}{n}\right) \\ &= (n\Delta\omega_v - \Delta\omega_s) - A\Delta\omega_s \end{aligned} \tag{33}$$

where $A = K_G/(1+\tau_d s)$-D_{pv}/n. Also, the relation of SG main driver droop governor is expressed as $K_G\Delta\omega_s = P_s{}^*-P_{ms}$, where P_{ms} is the mechanical power. Finally, the transient dynamic relationship is expressed as (34)

$$\begin{aligned} A\Delta\omega_s &\approx \frac{K_G}{\tau_{ds}}s\Delta\delta_2 - \frac{1}{n^2}(P_s^* - P_{ms}) \\ &= \frac{K_G}{\tau_d}\Delta\delta_2 - \frac{\Delta P_{ms}}{n^2} = \Delta P_s \end{aligned} \tag{34}$$

We introduce $\Delta P_v^* = \pm k^*\Delta\delta_s$, where k^* is the active power adjustment factor of VSG and also ΔP_v^* and $\Delta\delta_s$ are process variables. The value of ΔP_v^* should not exceed the ideal capacity of the system and should be maintained according to the equation (25). When $\Delta\delta_v$ and $\Delta\delta_s$ have opposite signs, the active power flows in the MG, and the negative sign is selected. And when $\Delta\delta_v$ and $\Delta\delta_s$ have the same sign, the load power changes, and the positive sign is selected. As a result, equation (34) is rewritten as (35):

$$\begin{aligned}(J_s\omega_n s + \frac{D_{pv}}{n})(n\Delta\omega_v - \Delta\omega_s) &= \Delta(P_s^* + P_s - P_v - P_v^*) \\ &= \Delta(P_s' - P_v) \mp k^*\Delta\delta_2 \end{aligned} \tag{35}$$

By different settings of k^*, an adjustment is made for governor inertia related to VSG and SG, which leads to robust operation in transient stability.

3) EXTRACTION OF PARAMETERS

By defining new variables in the form $\Delta\omega = n\Delta\omega_v - \Delta\omega_s$ and $\Delta\delta = n\Delta\delta_v - \Delta\delta_s$ and also paying attention to the fact that $\Delta\delta_s$ is much larger than $\Delta\delta_v$, the MG small signal model can be simplified as (36):

$$\begin{aligned}(J_s\omega_n s + \frac{D_{pv}}{n})\Delta\omega + 2M\Delta\delta \\ = 2M(n-1)\Delta\delta_v - k^*\Delta\delta_s \approx k^*\Delta\delta \end{aligned} \tag{36}$$

Based on this, the characteristic equation of the system can be expressed as (37):

$$G(s) = s^2 + \frac{D_{pv}}{J_s\omega_n n}s + \frac{2M + k^*}{J_s\omega_n} \tag{37}$$

According to the root-locus criterion, when it is $2M + k^* > 0$, the system has no specific roots with positive real parts and therefore is stable. But when it is sin $\theta z < 0$, the proposed power adjustment method is needed. Accordingly,

TABLE 2. Characteristics and parameters of the MG under study.

Parameters		Values
Nominal voltage of the DC grid side	VDC	400 V
Rated power of the DC/AC converter	PInverter	18KVA
PCC bus line-to-line voltage	VPCC	208 V
The switching frequency of each converter	FC	10KH
DC network loads in the order of number	PLoadi	1-2.5-0.75-1.8 KW
Capacitance of the DC link	Cpv	500μF
Resistance and inductance of BESS converter	Re and Le	50 mΩ and 2.5 mH
Current limitation of the battery converter	Imin and Imax	-40 A and +40 A
Capacity and virtual resistance of the battery	C and Rv	100 μf – 0.1Ω
Moment of inertia and virtual inertia	JS and JV	0.0898 kg.m2
Line impedances	ZV,ZLine-ZS	0.308+j0.708, 0.241+j0.828, 0.542+j0.591 Ω/10km
AC grid impedances	ZLine1,ZLine2	0.395+j0.644, 0.322+j0.624 Ω/15km
Rated power of induction motor 1	PIM1 and Cosθ	700 KW and 0.75 lag
Rated power of induction motor 2	PIM2 and Cosθ	5200 KW and 0.75 lag
Gains related to the BESS current controller	K1,K2,K3	-15.45,8.94,3,72
SOC controller gains	K1SOC,K2SOC	31.72,-25.21
Droop controller coefficients in VSG loop	Dpv, Dqv	850,290
Adjustment coefficients of controllers in AVR and GOV loop	KA, KG	17,31
Time constant of inertial response	dτ	0.5 s
Nominal angular frequency	ωn	314 rad/s
PREP modulation index	Km	42
Proportion factor of the phase controller	Kd	2.5

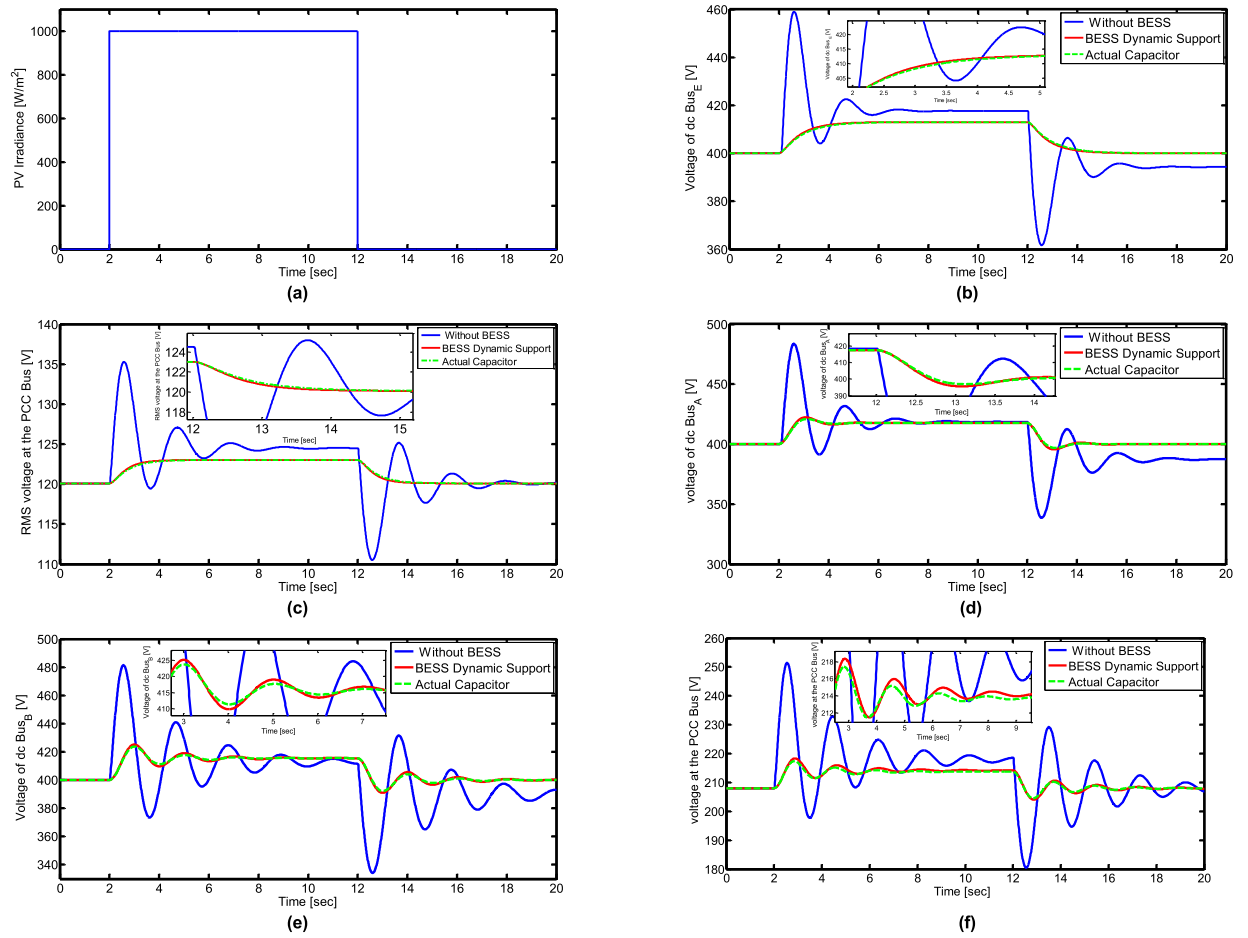

FIGURE 11. Simulation results related to the first scenario.

for the system to remain stable, the damping ratio is defined as (38):

$$\xi = \frac{D_{pv}}{n}\sqrt{\frac{Z_v Z_s Z}{J_s \omega_n (2E_v E_s sin\theta_z + k^* Z_v Z_s Z)}} \tag{38}$$

Figure 10 shows the poles of the closed-loop system based on the theory of the root-locus criterion of the roots to adjust the parameters. According to which, it can be seen that the damping ratio under constant D_{pv} and J_s is set at the optimal value of 0.65 to 0.85. Also, the value of $sin\theta z = -0.1$, the multiplier Z_vZ_sZ is equal to 5, the capacity ratio n is equal to 1, and k^* is set to 150, 220, and 290. According to Figure 8, it can be seen that the roots of the characteristic equation have the same distance from the real axis for different values. This means that the adjustment factor does not affect the stability of the whole system and only plays a significant role in adjusting the damping of the system. If it is chosen equal to 290, that is, A_3, the poles of the closed-loop system have an optimal damping ratio, and if it is chosen for 150, that is, A_1, and 220, that is, A_2, the oscillations of the system should increase. Therefore, with a compromise between the adjustment time and overshoot, the desired value can be extracted.

IV. SIMULATION RESULTS

To verify the proposed methods in BESS and VSG, simulations have been performed on an MG with SG and VSG units in MATLAB/Simulink and M-File environment. In the following, by defining different scenarios, the effectiveness of the proposed methods will be seen. The parameters of the system under study are collected according to Table 2.

First scenario: In this scenario, the results related to the design of the proposed controller in BESS considering the dynamic support when the static support is disabled ($K_b = 0$) are investigated. In order to compare the proposed controller, an actual capacitor (AC) has been used as a reference point and the state without the controller in BESS. In Figure 11(A), the PV radiation is shown, and based on the step jumps of the PV radiation at t = 2 seconds and t = 12 seconds, the output corresponding to the DC voltage of bus E in Figure 11(B) and the effective phase voltage of the bus PCC is shown in Figure 11(C). In Figure 11(D), the DC voltage of bus A with a power increase of 20 kW, and similarly in Figures 11(E) and 11(f), the results are related to the case where the load of 4.0 kW is connected to bus B at t = 2 and in t = 12 seconds is interrupted. From the results of this scenario, it can be seen that in the case without a compensator, with step jumps in PV radiation as well as the entry and exit of additional load, the

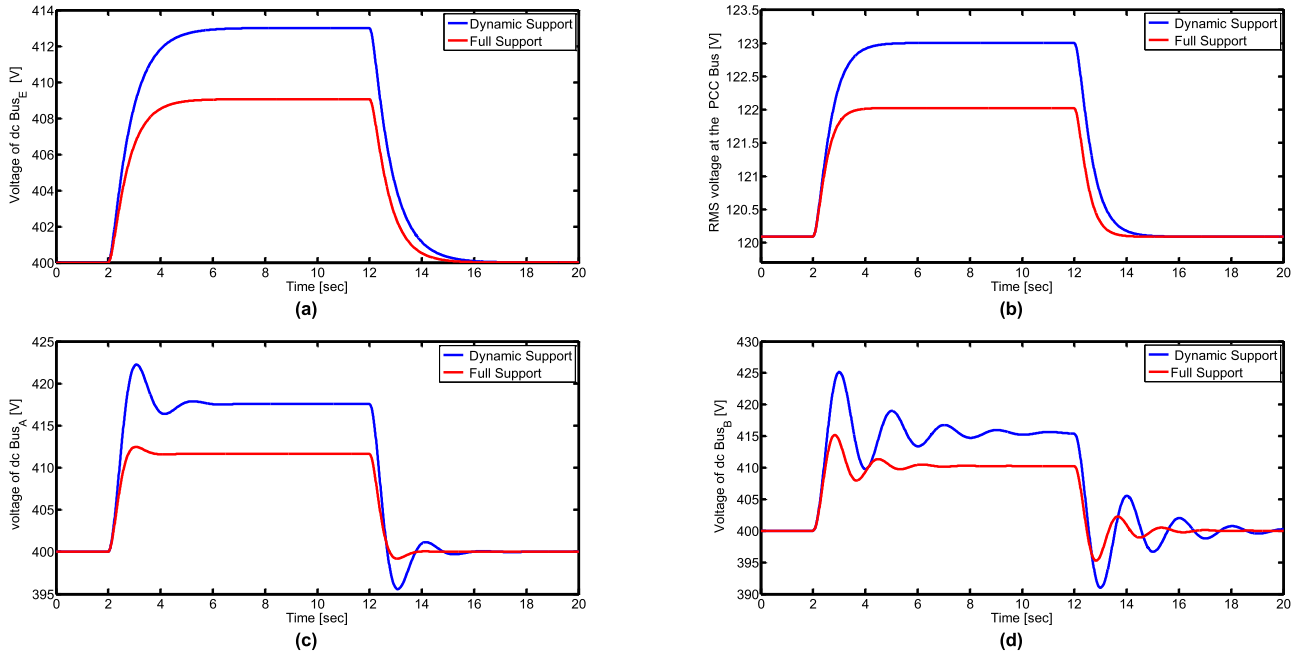

FIGURE 12. Simulation results related to the second scenario.

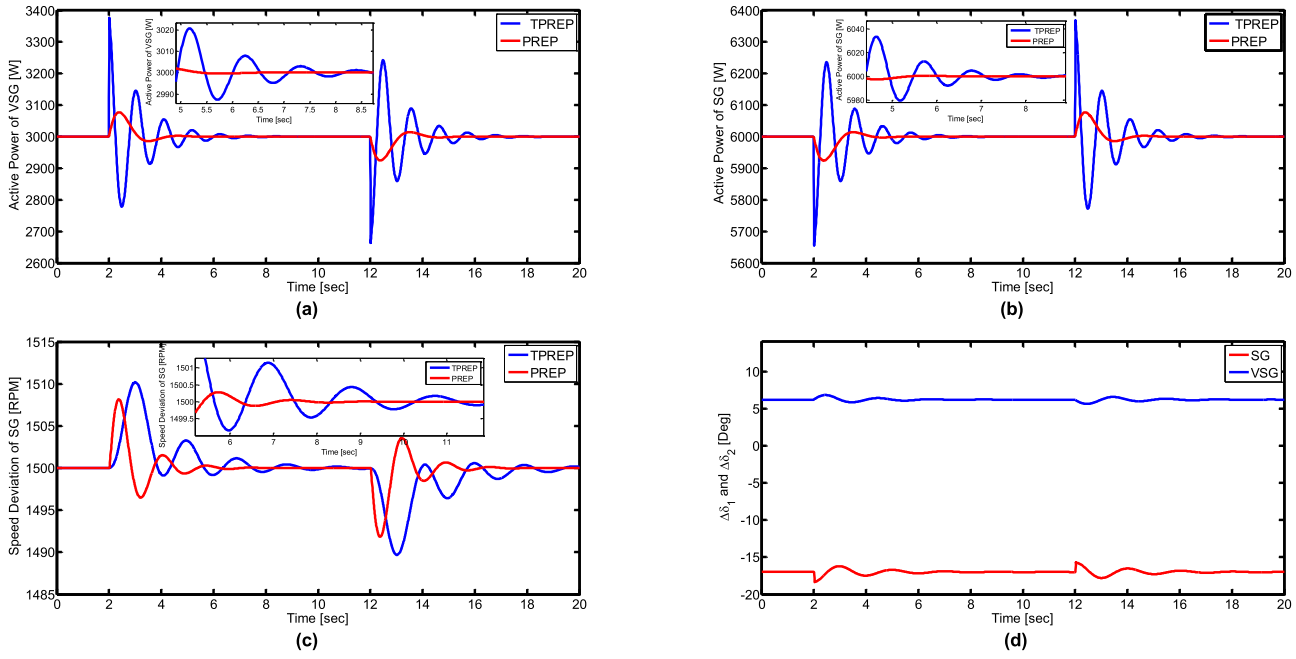

FIGURE 13. Simulation results related to the third scenario.

voltage in the DC bus and PCC undergoes fluctuations and offset. It is in this case that the proposed controller in BESS has been able to act like an actual capacitor by suppressing voltage fluctuations.

Second scenario: In this scenario, with the aim of full support for sudden changes of PV radiation at t = 2 and t = 12 seconds and setting the droop gain at the value of $K_b = 500$ (to activate the static support) the simulation results by providing responses based on support Dynamic alone and full support are shown in Figure 12. From the results of this scenario, it can be seen that with the activation of static support in BESS, when the voltage reaches the range of less than 400 V or more than 400 V, the corresponding compensation is done in the direction of power supply and power consumption, which leads to a very narrow range of voltage in jumps. It is caused by changes in PV radiation and load changes. In this scenario, the robust performance of the proposed controller in BESS is clearly seen

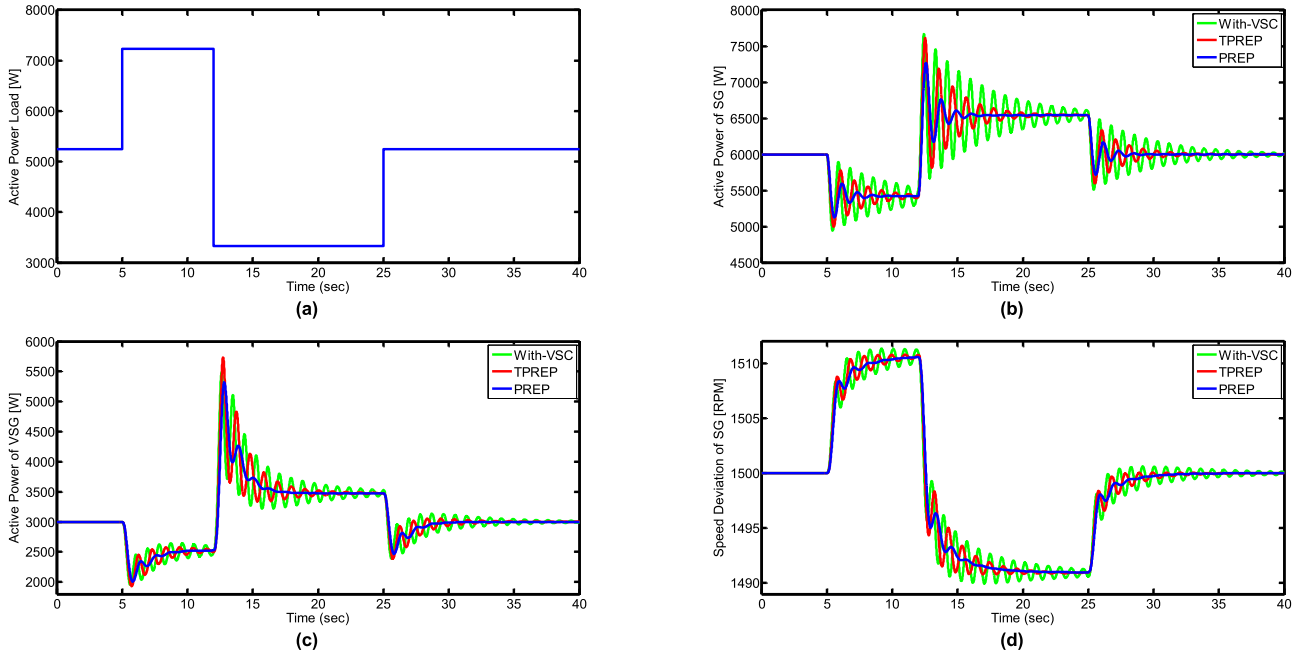

FIGURE 14. Simulation results related to the fourth scenario.

Third scenario: In this scenario, the transient performance of the system due to the closing of the power switch is checked by setting the active power factor in the value of $k^* = 290$, the ratio of the allocated capacity of VSG and SG is equal to 1:1 and n=1. Figures 13(a) and 13(b) show the active power changes for VSG and SG for the proposed method and the improved traditional method (TPREP), respectively. In Figure 13(c) for SG speed deviation changes, it can be seen that due to the delay in the inertia of the governor, the transient transfer time in the improved traditional method is always smooth with the delay, but in the proposed method, the transient fluctuations are quickly suppressed and the rotor speed in Optimal time reaches its synchronous state. Based on the proposed method in Figure 13(d) for power angle changes in SG and VSG, it can be seen that $\Delta\delta_s$ and $\Delta\delta_v$ have opposite signs, and therefore, the value of $\Delta P_v^* = -k^*\Delta\delta_s$ is selected to adjust the active power of VSG.

Fourth scenario: In this scenario, the simulation results by applying a temporary three-phase short-circuit fault on bus G in 5 seconds for 0.1 seconds, and also by adding an inductive load (induction motor 2) with a step diagram (according to Figure 14(a)), the simulation results are evaluated. Based on this, Figures 14(b) and 14(c) show the active power changes of SG and VSG for the PREP cases, the improved traditional method, and the case where the inverter-only DC/AC converter (With-VSC) is used, respectively. From these figures, it can be seen that the main driver of SG responds to the need to increase power, and at the same time, VSG also compensates for a part of the power gap and finally adapts to the inertia of the governor related shown for the three cases proposed in this scenario. It can be seen from the results of this scenario that in addition to fully compensating the inductive load under fault conditions, the SG and VSG synchronization functioned correctly and provided acceptable results for the system operation.

V. CONCLUSION

In this paper, a local robust controller was designed for BESS to perform the grid support level statically and dynamically by executing the commands issued from the secondary controller. This is intended to prevent overcurrent of the DC/DC converter during transient disturbances and to maintain the SOC state of the battery. Dynamic support is based on inertia modeled by a capacitor with capacitance C, and static support is modeled by a droop controller. In addition, to optimize the design of the gains related to the BESS controller, the LQR method was used to make the BESS performance more accurate and robust. In the following, VSG was used in parallel with SG to connect the PV converter connected to the AC grid to examine the coordination between power generation sources with different inertias and as a result, to adopt a suitable approach to improve the transient states caused by this exploitation. In this regard, a new parallelization method based on PREP for phase jump control and a method based on active power regulation in VSG were presented to improve the transient states caused by switching on and off the load, the presence of disturbances, and the existing inertia difference between SG and VSG. Therefore, a cosine function was used in the VSG active power loop to control the phase jump so that the frequency modulation signal without phase jump in each cycle enters the VSG-based inverter switching cycle.

In this method, the design of VSG and SG power angle coupling. was done by considering the capacity ratio of the units to lead to better frequency stability. The simulation

results were carried out by considering various uncertainties by MATLAB software, where the robust performance of the proposed controller was seen compared to other proposed methods.

Future research might investigate the adaptability of renewables and BESS in the large-scale power system and enhance the virtual inertia and frequency responses under the fluctuating power output. A comprehensive review of damping inertia control approaches, synthetic inertia control techniques, and VIC techniques can be adopted to enhance RESs power utilization. The authors aim to perform technical research by integrating intelligent techniques such as particle swarm optimization, genetic algorithm, etc., to maintain frequency and inertia responses optimally. The adaptation of power electronic converters to control the inertia responses under RESs connected microgrid can significantly contribute to this field of research.

REFERENCES

[1] M. Azimian, R. Habibifar, V. Amir, E. Shirazi, M. S. Javadi, A. E. Nezhad, and S. Mohseni, "Planning and financing strategy for clustered multi-carrier microgrids," *IEEE Access*, vol. 11, pp. 72050–72069, 2023.

[2] M. Darabian, A. Bagheri, and S. Behzadpoor, "A UPFC-based robust damping controller for optimal use of renewable energy sources in modern renewable integrated power systems," *IET Gener., Transmiss. Distrib.*, vol. 16, no. 20, pp. 4115–4131, Oct. 2022.

[3] F. G. Olanlari, T. Amraee, M. Moradi-Sepahvand, and A. Ahmadian, "Coordinated multi-objective scheduling of a multi-energy virtual power plant considering storages and demand response," *IET Gener., Transmiss. Distrib.*, vol. 16, no. 17, pp. 3539–3562, Sep. 2022.

[4] L. Peng, A. Zabihi, M. Azimian, H. Shirvani, and F. Shahnia, "Developing a robust expansion planning approach for transmission networks and privately-owned renewable sources," *IEEE Access*, vol. 11, pp. 76046–76058, 2022.

[5] S. Lin, Y. Wang, M. Liu, G. Fan, Z. Yang, and Q. Li, "Stochastic optimal dispatch of PV/wind/diesel/battery microgrids using state-space approximate dynamic programming," *IET Gener., Transmiss. Distrib.*, vol. 13, no. 15, pp. 3409–3420, Aug. 2019.

[6] J. H. Sanchez and L. M. Castro, "Advanced three-stage photovoltaic system phasor model for grid integration dynamic studies," *Sol. Energy*, vol. 235, pp. 82–93, Mar. 2022.

[7] U. G. Onu, G. S. Silva, A. C. Z. de Souza, B. D. Bonatto, and V. B. F. da Costa, "Integrated design of photovoltaic power generation plant with pumped hydro storage system and irrigation facility at the Uhuelem-Amoncha African community," *Renew. Energy*, vol. 198, pp. 1021–1031, Oct. 2022.

[8] X. Han, X. Li, and Z. Wang, "An optimal control method of microgrid system with household load considering battery service life," *J. Energy Storage*, vol. 56, Dec. 2022, Art. no. 106002.

[9] M. Azimian, V. Amir, S. Mohseni, A. C. Brent, N. Bazmohammadi, and J. M. Guerrero, "Optimal investment planning of bankable multi-carrier microgrid networks," *Appl. Energy*, vol. 328, Dec. 2022, Art. no. 120121.

[10] P. Balakumar, T. Vinopraba, S. Sankar, S. Santhoshkumar, and K. Chandrasekaran, "Smart hybrid microgrid for effective distributed renewable energy sharing of PV prosumers," *J. Energy Storage*, vol. 49, May 2022, Art. no. 104033.

[11] M. M. Rana, M. F. Romlie, M. F. Abdullah, M. Uddin, and M. R. Sarkar, "A novel peak load shaving algorithm for isolated microgrid using hybrid PV-BESS system," *Energy*, vol. 234, Nov. 2021, Art. no. 121157.

[12] K. Al-Khori, Y. Bicer, and M. Koç, "Comparative techno-economic assessment of integrated PV-SOFC and PV-battery hybrid system for natural gas processing plants," *Energy*, vol. 222, May 2021, Art. no. 119923.

[13] H. Nasrazadani, A. Sedighi, and H. Seifi, "Enhancing static voltage stability of a power system in the presence of large-scale PV plants using a battery energy storage control scheme by the probabilistic technique," *Int. J. Electr. Power Energy Syst.*, vol. 144, Jan. 2023, Art. no. 108517.

[14] X. Li, D. Hui, and X. Lai, "Battery energy storage station (BESS)-based smoothing control of photovoltaic (PV) and wind power generation fluctuations," *IEEE Trans. Sustain. Energy*, vol. 4, no. 2, pp. 464–473, Apr. 2013.

[15] A. Atif and M. Khalid, "Saviztky–Golay filtering for solar power smoothing and ramp rate reduction based on controlled battery energy storage," *IEEE Access*, vol. 8, pp. 33806–33817, 2020.

[16] S. Sukumar, M. Marsadek, K. R. Agileswari, and H. Mokhlis, "Ramp-rate control smoothing methods to control output power fluctuations from solar photovoltaic (PV) sources—A review," *J. Energy Storage*, vol. 20, pp. 218–229, Dec. 2018.

[17] Y. Yang, C. Li, J. Xu, F. Blaabjerg, and T. Dragicevic, "Virtual inertia control strategy for improving damping performance of DC microgrid with negative feedback effect," *IEEE J. Emerg. Sel. Topics Power Electron.*, vol. 9, no. 2, pp. 1241–1257, Apr. 2021.

[18] M. Eskandari, A. Rajabi, A. V. Savkin, M. H. Moradi, and Z. Y. Dong, "Battery energy storage systems (BESSs) and the economy-dynamics of microgrids: Review, analysis, and classification for standardization of BESSs applications," *J. Energy Storage*, vol. 55, Nov. 2022, Art. no. 105627.

[19] Z. Li, H. Li, X. Zheng, and M. Gao, "Virtual model predictive control for virtual synchronous generators to achieve coordinated voltage unbalance compensation in islanded micro grids," *Int. J. Electr. Power Energy Syst.*, vol. 146, Mar. 2023, Art. no. 108756.

[20] Y. Huo and G. Gruosso, "A novel ramp-rate control of grid-tied PV-battery systems to reduce required battery capacity," *Energy*, vol. 210, Nov. 2020, Art. no. 118433.

[21] K. Feng and C. Liu, "Multi-rate sampling control design and stability analysis for frequency and voltage regulation in islanded microgrids," *IEEE Trans. Sustain. Energy*, vol. 14, no. 1, pp. 704–716, Jan. 2023.

[22] N. S. Hasan, N. Rosmin, N. M. Nordin, S. A. Bakar, and A. H. M. Aman, "Dynamic response of hybrid energy storage based virtual inertial support in wind application," *J. Energy Storage*, vol. 53, Sep. 2022, Art. no. 105181.

[23] S. Chen, Y. Sun, H. Han, Z. Luo, G. Shi, L. Yuan, and J. M. Guerrero, "Active power oscillation suppression and dynamic performance improvement for multi-VSG grids based on consensus control via COI frequency," *Int. J. Electr. Power Energy Syst.*, vol. 147, May 2023, Art. no. 108796.

[24] X. Zhang, H. Liu, Y. Fu, and Y. Li, "Virtual shaft control of DFIG-based wind turbines for power oscillation suppression," *IEEE Trans. Sustain. Energy*, vol. 13, no. 4, pp. 2316–2330, Oct. 2022.

[25] A. Komijani, M. Sedighizadeh, and M. Kheradmandi, "Improving fault ride-through in meshed microgrids with wind and PV by virtual synchronous generator with SFCL and SMES," *J. Energy Storage*, vol. 50, Jun. 2022, Art. no. 103952.

[26] M. M. Mohamed, H. M. El Zoghby, S. M. Sharaf, and M. A. Mosa, "Optimal virtual synchronous generator control of battery/supercapacitor hybrid energy storage system for frequency response enhancement of photovoltaic/diesel microgrid," *J. Energy Storage*, vol. 51, Jul. 2022, Art. no. 104317.

[27] M. Li, Y. Wang, W. Hu, S. Shu, P. Yu, Z. Zhang, and F. Blaabjerg, "Unified modeling and analysis of dynamic power coupling for grid-forming converters," *IEEE Trans. Power Electron.*, vol. 37, no. 2, pp. 2321–2337, Feb. 2022.

[28] J. Fang, J. Zhao, L. Mao, K. Qu, and Z. Gao, "An improved virtual synchronous generator power control strategy considering time-varying characteristics of SOC," *Int. J. Electr. Power Energy Syst.*, vol. 144, Jan. 2023, Art. no. 108454.

[29] W. Xing, H. Wang, L. Lu, X. Han, K. Sun, and M. Ouyang, "An adaptive virtual inertia control strategy for distributed battery energy storage system in microgrids," *Energy*, vol. 233, Oct. 2021, Art. no. 121155.

[30] C. Wei, C. Tu, A. Wen, W. Song, and Q. Guo, "Coordinated voltage and island self-healing control of the BESS group," *Int. J. Electr. Power Energy Syst.*, vol. 142, Nov. 2022, Art. no. 108306.

[31] A. Ingalalli and S. Kamalasadan, "Decentralized state estimation-based optimal integral model predictive control of voltage and frequency in the distribution system microgrids," *IEEE Trans. Smart Grid*, vol. 14, no. 3, pp. 1790–1803, May 2023.

[32] B. Long, Y. Liao, K. T. Chong, J. Rodríguez, and J. M. Guerrero, "MPC-controlled virtual synchronous generator to enhance frequency and voltage dynamic performance in islanded microgrids," *IEEE Trans. Smart Grid*, vol. 12, no. 2, pp. 953–964, Mar. 2021.

[33] H. Cheng, Z. Shuai, C. Shen, X. Liu, Z. Li, and Z. J. Shen, "Transient angle stability of paralleled synchronous and virtual synchronous generators in islanded microgrids," *IEEE Trans. Power Electron.*, vol. 35, no. 8, pp. 8751–8765, Aug. 2020.
[34] A. D. Paquette, M. J. Reno, R. G. Harley, and D. M. Divan, "Sharing transient loads: Causes of unequal transient load sharing in islanded microgrid operation," *IEEE Ind. Appl. Mag.*, vol. 20, no. 2, pp. 23–34, Mar. 2014.
[35] Q. Lin, H. Uno, K. Ogawa, Y. Kanekiyo, T. Shijo, J. Arai, T. Matsuda, D. Yamashita, and K. Otani, "Field demonstration of parallel operation of virtual synchronous controlled grid-forming inverters and a diesel synchronous generator in a microgrid," *IEEE Access*, vol. 10, pp. 39095–39107, 2022.
[36] C. Li, Y. Cao, Y. Yang, J. Xu, M. Wu, W. Zhang, and T. Dragicevic, "New framework of RoCoF-FD for wideband stability evaluation in renewable energy generators with virtual impedance control," *IEEE Trans. Smart Grid*, vol. 13, no. 5, pp. 3570–3581, Sep. 2022.
[37] Q.-C. Zhong, P.-L. Nguyen, Z. Ma, and W. Sheng, "Self-synchronized synchronverters: Inverters without a dedicated synchronization unit," *IEEE Trans. Power Electron.*, vol. 29, no. 2, pp. 617–630, Feb. 2014.
[38] J. Liu, M. J. Hossain, J. Lu, F. H. M. Rafi, and H. Li, "A hybrid AC/DC microgrid control system based on a virtual synchronous generator for smooth transient performances," *Electric Power Syst. Res.*, vol. 162, pp. 169–182, Sep. 2018.
[39] R. Imran and S. Wang, "Enhanced two-stage hierarchical control for a dual mode WECS-based microgrid," *Energies*, vol. 11, no. 5, p. 1270, May 2018.
[40] M. Karimi-Ghartemani, S. A. Khajehoddin, P. Jain, and A. Bakhshai, "Linear quadratic output tracking and disturbance rejection," *Int. J. Control*, vol. 84, no. 8, pp. 1442–1449, Aug. 2011.
[41] I. Serban and C. Marinescu, "Control strategy of three-phase battery energy storage systems for frequency support in microgrids and with uninterrupted supply of local loads," *IEEE Trans. Power Electron.*, vol. 29, no. 9, pp. 5010–5020, Sep. 2014.

MOHANA ALANAZI received the B.Sc. degree (Hons.) in electrical engineering from the King Fahd University of Petroleum and Minerals, Saudi Arabia, in 2006, and the M.Sc. and Ph.D. degrees in electrical engineering from the University of Denver, Denver, CO, USA, in 2014 and 2019, respectively. He is currently an Assistant Professor with the Electrical Engineering Department, Jouf University, Saudi Arabia. His research interests include renewable energy integration, planning in power systems, microgrids, AI applications in power systems and forecasting, power optimization, and economic dispatch.

MOHAMED SALEM (Member, IEEE) received the B.Eng. degree in electrical and power engineering from Elmergib University, Al Khums, Libya, in 2008, the M.Sc. degree in electrical engineering from the Tun Hussein Onn University of Malaysia (UTHM), Batu Pahat, Johor, Malaysia, in 2011, and the Ph.D. degree from the Department of Power Engineering, Faculty of Electrical Engineering, Universiti Teknologi Malaysia (UTM), Malaysia, in August 2017. He has been a Senior Lecturer with the School of Electrical and Electronic Engineering, Universiti Sains Malaysia (USM), Penang, Malaysia, since July 2018. He has authored or coauthored number of well recognized journal articles and conference papers. His research interests include dc–dc converter, renewable energy applications, energy conversion, and control of power electronics systems. He is a member of IES. He has served as a guest editor for various special issues. He is a registered Graduate Engineers Malaysia (BEM) in the electrical track.

MOHAMMAD HOSEIN SABZALIAN was born in Iran. He received the Ph.D. degree in Control Science and Engineering from Shanghai Jiao Tong University (SJTU), China. He was a postdoctorate fellow at the Federal University of Rio de Janeiro (UFRJ) and University of Campinas (UNICAMP) using International CAPES and the matic International and multidisciplinary FAPESP scholarships in Brazil respectively (2021–2023). Currently, he is working as an Assistant Professor at the Mechatronics groups, Department of Mechanical Engineering, University of Santiago of Chile, (USACH), Chile. His research interests include control theory, intelligent control, machine learning, fuzzy systems, adaptive control, nonlinear control, and their applications in several fields, including renewable energy, automatic vehicles, chaotic systems, mechatronics and robotics systems.

NATARAJAN PRABAHARAN (Senior Member, IEEE) received the B.E. degree in electrical and electronics engineering and the M.E. degree in power electronics and drives from the Affiliated College, Anna University, Chennai, India, in 2012 and 2014, respectively, and the Ph.D. degree in energy and power electronics from the Vellore Institute of Technology (VIT) University, Vellore, India, in 2017. He is currently an Assistant Professor with the Department of Electrical and Electronics Engineering, SASTRA Deemed to be University, Thanjavur, India. His research interests include power electronics, new topologies for inverter and converters, energy trading, electric vehicle, demand side management, grid integration of renewable energy sources and its controllers, photovoltaic systems, and microgrid. He is a technical program committee member of many reputed international conferences. He was a recipient of the University Merit Ranker Award, in 2014. He was a recipient of two prestigious travel grants under the category of Young Scientist from the Science and Engineering Research Board and Asian Development Bank, in 2015 and 2016, respectively. He has received the Outstanding Editorial Board Member Award in *ITEES* (Wiley), in 2020 and 2021. He serves as an Associate Editor for the *IET Renewable Power Generation*, *International Transactions on Electrical Energy Systems*, IEEE Access, *Journal of Power Electronics*, and *International Journal of Renewable Energy Research*.

SOICHIRO UEDA (Student Member, IEEE) received the B.Eng. degree in electrical systems engineering from the University of the Ryukyus, Japan, in 2022, where he is currently pursuing the M.Eng. degree. His research interests include renewable energy, energy management, microgrid, and model predictive control.

TOMONOBU SENJYU (Fellow, IEEE) received the B.S. and M.S. degrees in electrical engineering from the University of the Ryukyus, in 1986 and 1988, respectively, and the Ph.D. degree in electrical engineering from Nagoya University, in 1994. Since 1988, he has been with the Department of Electrical and Electronics Engineering, Faculty of Engineering, University of the Ryukyus, where he is currently a Professor. His research interests include power system optimization and operation, advanced control, renewable energy, the IoT for energy management, ZEH/ZEB, smart city, and power electronics. He is a fellow of IEEJ and AAIA.